A Novel Nomogram Combined With Radiomics Features, Age and Albuminuria to Predict the Pathological Grade of Bladder Cancer Running Title: Application Study on the Prediction Model of Bladder Cancer Pathological Grade Based on Parameters of Thin-layer Enhanced CT. Author Information

Qi Zhou
the First Affiliated Hospital of Soochow University
Lu Ma
the First Affiliated Hospital of Soochow University
Haoyang Zhang
the First Affiliated Hospital of Soochow University
Xiaojie Ang
the First Affiliated Hospital of Soochow University
Can Hu
the First Affiliated Hospital of Soochow University
Caiping Mao
the First Affiliated Hospital of Soochow University
Zhiyu Zhang
the First Affiliated Hospital of Soochow University
Jun Ouyang (ouyangjun99@sina.com)
the First Affiliated Hospital of Soochow University

Research Article

Keywords: Bladder Cancer, Pathological grade, Radiomics, Texture feature, Nomogram

Posted Date: September 27th, 2021

DOI: https://doi.org/10.21203/rs.3.rs-891133/v1

Abstract

Background: Based on multi-parameter thin-slice enhanced CT texture features and related clinical indicators, a preoperative pathological grade prediction model of bladder urothelial carcinoma was established.

Methods: The CT images and clinical data of 372 patients with urothelial carcinoma in our hospital from January 2015 to October 2020 were collected. 372 patients were divided into two groups: HGUC(n=190) and LGUC(n=182). All patients were divided into 10 groups on average, of which 7 were used as training group (n=259) and the remaining 3 as verification group (n=113). Then, by using 3D-Slicer software from all enhanced in patients with preoperative CT images (Arterial and Venous phase calibration chart) split out the region of interest (ROI), respectively from the tumor image data extraction based on First-order and Second-order, High-order and filtering characteristics of 1223 texture features, and use the inter/intra-class correlation coefficient(ICC > 0.75) between classes and least absolute shrinkage selection operator (LASSO) regression feature selection; Secondly, the clinical effective factors were obtained by logistic regression analysis, and the clinical predictive model was constructed. Finally, the selected clinical key indicators and radiomics features were mapped. In order to verify the predictive ability of the nomogram, conformance index (C-index), calibration curve, Receiver operator characteristic (ROC) curve and clinical decision curve analysis (DCA) were used to test the nomogram.

Results: Lasso regression analysis showed that 11 radiomics features were significantly correlated with the pathological grade of bladder cancer. After comparing the four models, it is found that Logistic regression model has the best prediction ability (AUC=0.858). The results of multivariate analysis showed that age and albuminuria were independent influencing factors. A comprehensive model for predicting the pathological grade of bladder cancer (radiomics + clinical) was constructed by combining clinical independent risk factors with 11 radiomics features. Compared with clinical feature model and radiomics model, it was found that the predictive performance of imaging comprehensive model combined with clinical factors was the best (AUC=0.864).

Conclusions: The radiomics model based on multi-parameter thin-layer enhanced CT, combined with clinical factors, can effectively predict high-and low-grade urothelial carcinoma.

Introduction

Bladder Cancer (BCa) is one of the most common malignant tumors in the urinary system (1). More than 95% of bladder cancers are urothelial cancers, and non-muscle invasive bladder cancer (NMIBC) accounts for 75–80% of urothelial cancers, including confined to the mucosa (Ta, carcinoma in situ) or submucosa (T1) (2). Especially in the past few decades, the incidence and mortality of bladder cancer in China have been increasing rapidly (3). Although current therapies for bladder cancer have improved, the prognosis of bladder cancer patients is still poor (4). In addition, the urban prevalence of bladder cancer is higher than in rural areas (5).

The pathological grading of bladder cancer is one of the most important reference factors for the treatment and prognosis of patients with bladder cancer. Accurately predicting the pathological grading before surgery is crucial to the choice of treatment options (6-7). High-grade urothelial carcinoma (HGUC) is more likely to progress to muscle invasion and has a higher recurrence rate (8-9). The probability of progression of low-grade urothelial carcinoma (LGUC) in stage Ta is about 6%, while the probability of progression in HGUC in stage T1 reaches 17% (10-11). Patients with LGUC are the best candidates for bladder infusion chemotherapy after preventive transurethral resection (12). For patients with HGUC, not only need to undergo bladder infusion chemotherapy within 1 to 3 years, but also consider radical cystectomy if necessary (13). The classification of bladder cancer is mainly based on the pathological diagnosis after biopsy. At present, the preoperative pathological classification of bladder cancer mainly relies on cystoscopy for tissue biopsy, but cystoscopy biopsy is an invasive examination, and there is a risk of urinary tract infection and injury (14). Therefore, there is an urgent need to explore a new, non-invasive method for predicting pathological grading before surgery, which can help clinicians to

make preliminary inferences about the pathological grading of patients before surgery, and is helpful for personalized treatment and treatment of patients with bladder cancer. It is helpful for personalized treatment and management of bladder cancer patients.

After more than ten years of development, medical imaging technology is not only a diagnostic tool, it has become the key to tumor diagnosis, treatment, and disease evaluation (15). Medical imaging technology is playing an increasingly important role in all stages of cancer treatment (16-18). Imaging technology is not only used in the prediction of tumor recurrence and diagnosis, but also can achieve a good predictive effect in preliminary screening, biopsy guidance and pathological staging, and even has a certain effect in patient prognosis assessment and pain relief (19-28). At present, CT imaging technology has been applied to all stages of cancer management and plays a pivotal role. However, CT imaging cannot describe the internal features or molecular details of solid tumors (29-30). In addition, the current main imaging technologies also include dynamic contraction-enhanced magnetic resonance imaging (DCE-MRI) and positron emission tomography (PET), etc. They are more effective in the identification and progress assessment of tumor tissues.

In recent years, image texture analysis technology has been used to dig out a large number of relevant characteristic parameters from medical imaging data of specific cancers to assist clinical and radiologists in accurate cancer diagnosis and assessment, and obtain useful information that cannot be seen by the naked eye, becoming mainstream (31-33). Radiomics was originally proposed by Dutch scholars. It extracts high-throughput image features through image analysis technology, converts them into computable spatial texture data, and uses supervised or unsupervised methods to classify textures to make them has a strong ability to quantify heterogeneity (34). At present, many studies have shown that the combination of radiomics and machine learning algorithms have shown good performance in the differential diagnosis and staging prediction of diseases (35). Although the role of magnetic resonance imaging (MRI) in the diagnosis and progression assessment of bladder cancer has been reported (36). However, conventional images with echo-planar magnetic resonance sequences cannot identify the primary tumor well, and may be inaccurate in identifying the local stage. In addition, MRI examination also has the disadvantages of longer time, higher economic cost, and more scanning parameters, however, the CT examination time is short, the cost is low, and the thin-layer CT enhanced image can show the lesion more clearly, and it is not easy to cause the omission of edge texture information (37).

In recent years, radiomics proposed by many research scholars plays different roles in a variety of tumors, and has become a hot spot in medical research, and has great potential in the diagnosis, pathology and progression prediction of bladder tumors (38-43). Computerized tomography (CT) examination is the most commonly used preoperative diagnosis and evaluation method for patients with bladder cancer, it is used to locate the tumor and determine the number and size of the lesions, at the same time, it can also make a certain preliminary judgment on the degree of tumor invasion and metastasis, but the internal characteristics of the tumor cannot be directly obtained with the naked eye, and image texture feature analysis can further explore the morphology and internal texture information of the tumor (44-45). At present, there are few literature reports on predicting the pathological grading of bladder cancer, and most of them are small in sample size, poor in comprehensive performance, and not combined with clinically relevant factors, so the clinical application is not high. This research aims to find characteristic texture parameters from multi-parameter thin-layer enhanced CT through texture analysis technology, and combine machine learning algorithms to achieve the purpose of non-invasive and quantitative prediction of the pathological grade of bladder cancer before surgery. In addition, on this basis, we tried to develop the nomogram and apply it to the clinic, which included radiomics features and clinical risk factors.

Materials And Methods

Data of patients

This study collected a total of 372 patients who underwent surgical treatment in our hospital's urology department from January 2015 to October 2020 and were pathologically diagnosed as urothelial carcinoma after surgery. Among them,

there were 182 cases and 190 cases of low-grade urothelial carcinoma and high-grade urothelial carcinoma, respectively.

Selection criteria

Inclusion criteria

(1) Pathological diagnosis of urothelial carcinoma after transurethral resection of bladder tumor or total cystectomy during hospitalization, complete clinical data and complete pathological report; (2) Thin-layer enhanced CT of the bladder within one month, and the bladder is well filled, with complete imaging data; (3) Bladder tumor diameter>=1cm;

Exclusion criteria

(1) Those undergoing neoadjuvant treatment with bladder perfusion or intravenous chemotherapy before surgery; (2) Insufficient bladder filling and tumor minimum diameter <1cm (including squamous carcinoma); (3) Patients with insufficiency of important organs; Patients with inflammatory bladder diseases and mental disorders; (5) Patients with other malignant tumors; A total of 372 patients were enrolled and were randomly divided into training and verification groups according to the proportion of 7:3. The patient recruitment pathway is shown in **Fig.1.**

Methods

Clinical data and image data collection

The clinical data includes the patient's height, age, gender, urinary PH, weight, metabolic syndrome (MS), high blood pressure (HBP), urinary tract infection, body mass index (BMI), hematuria, albuminuria, high-density lipoprotein (HDL-C), tumor location, tumor number, tumor size (maximum diameter), diabetes mellitus (DM), Triglyceride (TG), pathological grade, past history and family history, etc. The patient’s imaging data includes: thin-layer CT images of the venous phase and arterial phase within one month before the operation, and the image quality is good, and the bladder tumor is clearly imaged without artifacts.

CT scanning method

All patients underwent Siemens 64-slice spiral CT bladder-enhanced examination in our hospital. After the image is reconstructed, it is uploaded to the picture archiving and communication system (PACS) imaging system in uncompressed digital imaging and communications in medicine (DICOM) format, and all the patient's arterial phase and venous thin layer image data are downloaded from the PACS system.

Delineation of image ROI

First, import the arterial and venous thin-layer images of the lesion into the 3D-Slicer image editing software. In order to reduce the influence of changes in contrast and brightness on the texture analysis results, the arterial and venous images are uniformly calibrated and merged into an image of arteriovenous phase fusion. Two residents with more than three years of experience in urinary system imaging diagnosis applied the hidden density processing (Threshold) function and the Sphere brush function in the texture analysis 3D-Slicer software when the pathological results were unknown. The continuous-level semi-automatic ROI is delineated for bladder tumor lesions. In order to unify the shape of the ROI cut from each tumor, smoothing is performed. The specific process is shown in **Fig.2.** In addition, in order to delineate the entire bladder tumor as completely as possible, try to keep the delineation line about 1-2mm away from the edge of the tumor. For multiple foci, considering the heterogeneity among different individuals, only the largest foci were included in the study.

Image processing and data acquisition

The complete tumor ROI is obtained by semi-automatic delineation. In order to transform the tumor ROI into visual data for analysis, a series of processing of the tumor ROI is required, parameters are set, and the original data required for the research is obtained. Select the Radiomics function of the 3D-Slicer software to perform a series of data analysis and processing on the tumor ROI outlined in the previous stage, and select the radiomics texture features we need. The feature parameters include: First-order, Shape features (shape2D, shape3D), gray-level run-length matrix (GLRLM), gray-level dependence matrix (GLDM), gray-level size zone matrix (GLSZM), neighboring gray-tone difference matrix (NGDTM) and gray-level co-occurrence matrix (GLCM) and filtering characteristics. Set resampling and filtering criteria were as follows: resampled voxel size (1, 1, 1), LoG kernel sizes (1, 1.5, 2, 2.5), and wavelet-based features. For multiple lesions, considering the heterogeneity among different individuals, only the most significant lesions were included.

Texture feature data preprocessing

The process is mainly operated by 3D-slicer software (www.slicer.org/) to extract effective features from tumor image data. Finally, the Radiomics package is used to extract three-dimensional (3D) radiomics features, including first-order features, second-order features, high-order features and filtering features (41, 43, 46-47). Among them, the first-order features are mainly used to describe the global features related to the frequency distribution of image gray levels, such as Energy, etc; The second-order features are mainly used to describe the local distribution characteristics of image gray levels, such as Autocorrelation, Contrast, Correlation, Difference Average and Difference Entropy; High-level features describe the gray-scale regional distribution characteristics of the image, such as Coarseness and Complexity; This study extracts a total of 80 types of features from tumor ROI, including First-order features (18 types), Shape features (3D) (16 types), Shape features (2D) (14 types), GLCM (24 types), GLRLM (16 types), GLSZM (16 types), NGDTM (5 types), and GLDM (14 types), total extracted 1223 radiomics features. In order to facilitate the subsequent calculation and analysis, the characteristics are numbered and assigned, which are sequentially numbered X1, X2...X1223. The preprocessing of the characteristic data is essential. The first is to process all the null values and replace them with the median. Then the extracted texture parameters are screened by the correlation coefficient between groups (ICC>0.75). In order to facilitate subsequent calculation and display, the feature is reduced by Z-score, so that the feature value is between [-1,1] after being reduced in dimension.

Texture feature extraction and screening

Selection operator (LASSO) regression method selects effective radiomics features from the training group. Logistic regression, decision tree, support vector machine (SVM) and adaptive boosting (Adaboost) are used for model construction, and accuracy, sensitivity, specificity and area under the curve (AUC) are used as model evaluation indicators.

Selection and assignment of clinical related factors

In order to construct a predictive model of the pathological grade of bladder cancer, and make the model more perfect and efficient. We add gender, age, height, weight, HBP, urine pH, urinary tract infection, hematuria, albuminuria, HDL-C, tumor location, tumor number, tumor size (maximum diameter), DM, TG, pathological grade, MS, past history and family history and other clinical characteristics. Considering that this research requires a lot of data and complicated parameters, in order to improve the calculation efficiency and intuitive display, all the parameters participating in the research are assigned. For example, low-grade urothelial carcinoma (LGUC) is assigned a value of "0" during classification, otherwise, it is marked as "1". Refer to **Table 1** for the assignment of other clinical related factors.

Table 1. Clinical factor assignment.

Clinical factor	Assignment“0”	Assignment“1”
Gender	Female	Male
Urinary tract infection	No	Yes
Hematuria (%)	No	Yes
Proteinuria	No	Yes
Number	Single	Multiple (>=2)
Metabolic syndrome (MS)	No	Yes
BMI	BMI<25	BMI≥25
Triglyceride	<1.7	≥1.7
High blood pressure (HBP)	No	Yes
Diabetes mellitus (DM)	No	Yes

Definition: yes=1,no=0. BMI normal value=18.5-23.9. Triglyceride normal value=0.45□1.69mmol/L. High-Density Lipoprotein(HDL) normal value=0.7□2.0mmol/L. Urine PH normal value=6.0-6.5

Predictive model construction (comparison of four algorithm models)

First, build four prediction models for bladder cancer pathology classification on the already divided training group. By comparing accuracy, sensitivity, specificity and AUC select the radiomics feature prediction model with the highest prediction efficiency. In order to verify the predictive capabilities of the four predictive models, this study uses a 10-fold cross-validation method and performs 100 iterations; at the same time, it compares with the clinical feature prediction model based on clinical feature indicators and selects a model with better predictive capability.

Statistical software and methods

The software used in this study included 3D-Slicer (4.10.2-Win-amd 64), R-Studio (1.2.1335), and related software packages. The clinical-related factors were analyzed using SPSS22.0 software (IBM), and the measured data was expressed as x ± s. T-test was used to compare the two groups of measurement data, and the counting data was compared by chi-square test. Independent risk factors were found by logistic regression. We compared the values of radiological features in the differential diagnosis of LGUC and HGUC using a single-factor analysis of variance. The LASSO regression model was analyzed using the "glmnet" software package. We used the "proc" software package to draw ROC curves. The differences in AUC values among models were tested using the Delong test. P<0.05 (two-sided) was considered to indicate significance. The effectiveness of the model is expressed by the C-index, and the model is verified by the decision curve (DCA).

Results

Correlation analysis of clinical features

A total of 372 patients with bladder cancer were included in this study. The basic information includes height, age, gender, urinary PH, weight, MS, HBP, urinary tract infection, BMI, hematuria, proteinuria, HDL-C, tumor location, tumor number, tumor size (maximum diameter), DM, TG, pathological grade, past history and family history, etc. Among them, 301 were males and 71 were females; aged 26 to 95 years, with an average of 65.48±12.39 years), including 182 cases of LGUC and 190 cases of HGUC. The characteristics of the high- and low-level groups and the entire patient group are shown in **Table 2**. According to the ratio of 7:3, the patients were randomly divided into training group (n=259) and verification group

(n=113). In the training group and the verification group, the information of HGUC and LGUC patients is shown in **Table 3**. Univariate analysis showed that factors such as age, urinary tract infection, hematuria, albuminuria and tumor diameter were statistically significant (p<0.05). Multivariate analysis showed that in the clinical prediction model, age and proteinuria were still independent risk factors (p<0.01).

Table 2. General information of patients in training group and verification group.

Clinical factor	*LGUC（N=182）*	*HGUC（N=190）*	*U/c²*	*P*
Age (c±S, year)	61.98±12.29	68.85±11.91	11574	**<0.0001**
Gender (%)			2.733	0.0983
Male	141(77.5%)	160(84.2%)		
Female	41(22.5%)	30(15.8%)		
BMI (c±S, kg/m²)	23.56±3.275	23.42±3.243	17190	0.9235
Urine PH (c±S)	6. 052±0.7187	6.079±0.7376	16860	0.6699
Urinary infection (%)			13.78	**0.0002**
Yes	81(44.5%)	121(63.7%)		
No	101(55.5%)	69(36.3%)		
Hematuria (%)			18.44	**<0.0001**
Yes	105(57.7%)	149(78.4%)		
No	77(42.3%)	41(21.6%)		
Proteinuria (%)			42.12	**<0.0001**
Yes	52(28.6%)	118(62.1%)		
No	130(71.4%)	72(37.9%)		
Tumor location (%)			6.487	0.2617
Left side wall	69(37.9%)	86(46.8%)		
Right side wall	49(26.9%)	55(28.9%)		
Bladder triangle	12(6.6%)	9(4.7%)		
Front wall	7(3.8%)	11(5.8%)		
Posterior wall	39(21.4%)	25(13.2%)		
Bladder vault	5(3.4%)	4(6%)		
Tumor number (%)			0.4112	0.5213
single	162(89%)	165(86.8%)		
Multiple (>=2)	20(11%)	25(13.2%)		
Tumor size (c±S, mm)	19.65±11.27	24.94±15.05	13804	**0.0007**
MS (%)			0.4207	0.5166
Yes	50(27.5%)	58(30.5%)		
No	132(72.5%)	132(69.5%)		
HBP (%)			1.210	0.2714
Yes	74(40.7%)	88(46.3%)		
No	108(59.3%)	102(53.7%)		

Clinical factor	*LGUC（N=182）*	*HGUC（N=190）*	*U/c²*	*P*
Triglycerides (c±S)	1.443±0.8769	1.415±0.8038	16390	0.3853
HDL-C (c±S)	1.201±0.3570	1.204±0.3159	16933	0.7305
DM (%)			2.599	0.1070
Yes	30(16.5%)	44(23.2%)		
No	152(83.5%)	146(76.8%)		

Bold values indicate significant difference.

LGUC = Low-grade urothelial carcinoma; HGUC = Low-grade urothelial carcinoma; BMI = Body mass index; MS = Metabolic syndrome; HBP = high blood pressure; HDL-C = High density lipoprotein cholesterol; DM = Diabetes mellitus

Table3. Comparison of the characteristics of HGUC and LGUC in the training group and the training group.

Clinical factor	*Training group (259)*		*U/χ2*	*P*	Validation *group (113)*		*U/χ2*	*P*
	HGUC (126)	*LGUC (133)*			*HGUC (64)*	*LGUC (49)*		
Age (*c±S*, year)	68.83±12.07	61.53±12.61	5656	**<0.0001**	68.91±11.68	63.20±11.43	1046	**0.002**
Gender (%)			0.735	0.39			2.746	0.097
Male	103	103			57	38		
Female	23	30			7	11		
BMI (c±S, kg/m^2)	23.42±3.37	23.28±3.12	8133	0.68	23.44±2.99	24.32±3.58	1401	0.335
Urine PH (c±S)	6.04±0.67	6.06±0.73	8368	0.98	6.14±0.71	6.02±0.66	1446	0.467
Urinary infection (%)			14.62	0.0001			5.470	0.019
Yes	82	55			44	23		
No	44	78			20	26		
Hematuria (%)			21.43	**<0.0001**			7.846	**0.005**
Yes	103	64			51	27		
No	23	69			13	22		
Proteinuria (%)			34.71	<0.0001			7.942	0.004
Yes	80	36			38	16		
No	46	97			26	33		
Tumor location (%)			4.755	0.446			9.543	0.089
Left side wall	59	53			27	16		
Right side wall	37	32			18	17		
Bladder triangle	7	11			2	1		
Front wall	4	7			7	0		
Posterior wall	17	26			8	13		
Bladder vault	2	4			2	2		
Tumor number (%)			0.690	0.405			3.205	0.073
single	114	116			51	45		
Multiple (>=2)	12	17			13	4		
Tumor size (c±S, mm)	25.30±15.62	18.57±9.82	6320	0.0006	28.20±15.99	21.76±12.11	1206	0.035
MS (%)			0.302	0.582			0.094	0.758
Yes	38	36			20	14		

No	88	97			44	35		
HBP (%)			0.378	0.5385			0.0029	0.956
Yes	54	52			34	30		
No	72	81			30	27		
Triglycerides (c±S)	1.42±0.80	1.46±0.97	7996	0.525	1.40±0.81	1.37±0.54	1455	0.513
HDL-C (c±S)	1.21±0.31	1.23±0.38	8332	0.937	1.18±0.31	1.11±0.23	1465	0.553
DM (%)			0.709	0.399			0.430	0.511
Yes	48	44			22	14		
No	78	89			42	35		

Bold values indicate significant difference. P<0.01 considered statistically significant.

Selection of radiomics features

Among the 1223 radiomics features extracted from CT images (after calibration in the arteriovenous phase), 669 proved to have good inter-group and intra-class consistency (ICC>=0.75), ICC (mean=0.748, median=0.807) **(Fig.3a).** Through one-way analysis of variance, 651 radiomics features are significantly different between HGUC and LGUC (*p<0.05*), and enter the LASSO regression model to select the most valuable features **(Fig.3b)**. Select the most valuable features, use the minimum criterion for 10 cross-validation, and finally get 11 valid features to build the predictive model (**Fig.3b and Fig.3c**). This process mainly uses the “p-ROC” and “glmnet” R packages.

Construction and selection of Model

We use 11 effective features to build models, and try to build four models based on the training group: Logistic regression model, SVM, ADABOST and decision tree model. We found that only the logistic regression model is the most valuable. The AUC values of Logistic regression, decision tree, SVM, and ADABOST models based on the training group are 0.858, 0.872, 0.852 and 0.789, respectively. The sensitivity, specificity, and accuracy of the training group of the Logistic regression model are 75.40%, 82.71% and 79.15%, respectively, (95%CI: 0.812-0.903), and the verification group were 76.36%, 68.97% and 72.57%, respectively, (95%CI: 0.719-0.881). Decision tree prediction models were 80.16%, 87.22%, 83.79% (95%CI: 0.829-0.914) and 74.55%, 72.41%, 73.45% (95%CI: 0.573-0.784); SVM prediction model were 65.08%, 85.71%, 75.68% (95%CI: 0.806-0.989) and 65.45%, 72.41%, 69.03% (95%CI: 0.729-0.887). The ADABOST prediction models were 84.92%, 72.93%, 78.76% (95% CI: 0.740-0.839) and 85.45%, 53.44%, 69.03% (95% CI: 0.615-0.775). A comprehensive comparison of these four prediction models shows that the comprehensive diagnosis effect based on the logistic regression algorithm is the best, not only has a good AUC value in the training group, but also can be well verified in the verification group. The accuracy, sensitivity, specificity and AUC of the training group and the verification group are balanced. The AUC values of the logistic regression prediction model training group and verification group were 0.858 and 0.800, respectively (**Fig.4**). Comparing the performance of the four models, it can be seen that the radiomics model based on the logistic regression model has good performance in terms of accuracy, specificity, sensitivity and AUC, and the overall performance is better. There are significant differences between HGUC and LGUC. **Table4** summarizes the diagnostic performance of each algorithm model.

Table 4. Comparison of four algorithm models based on the training group.

Algorithm models	Group	Accuracy (%)	Sensitivity (%)	Specificity (%)	95% CI	AUC
Logistic regression	Train	79.15	75.40	82.71	0.812-0.903	0.858
	Test	72.57	76.36	68.97	0.719-0.881	0.800
Decision tree	Train	83.79	80.16	87.22	0.829-0.914	0.872
	Test	73.45	74.55	72.41	0.573-0.784	0.679
SVM	Train	75.68	65.08	85.71	0.806-0.898	0.852
	Test	69.03	65.45	72.41	0.729-0.887	0.808
ADABOST	Train	78.76	84.92	72.93	0.740-0.839	0.789
	Test	69.03	85.45	53.44	0.615-0.775	0.695

SVM = support vector machine; ADABOST = adaptive boosting.

Model construction and evaluation

Through univariate and multivariate analysis, it was found that age and proteinuria were independent risk factors for the pathological grading of bladder cancer patients. It can be concluded that patients with symptoms of albuminuria before surgery have a greater risk of HGUC. In addition, age is also related to pathological grading. The older the age, the greater the risk of HGUC. In the training group, a clinical prediction model was established based on two risk factors and compared with the radiomics model. In the training group, the AUC values of the radiomics model and the clinical prediction model were 0.858 and 0.650, respectively. There are obvious differences between the two models (p=0.001). The ROC curves of the two models and the comprehensive model are shown in **Fig.5**. By comparison, it can be seen that the predictive performance of the radiomics model is significantly greater than that of the clinical predictive model, and it has better performance in predicting the pathological grade of bladder cancer. In addition, we added clinical factors to the radiomics model to obtain a comprehensive model (radiomics + clinical), and found that its predictive performance was slightly higher than that of the radiomics model (AUC=0.864).

The establishment of radiomics nomogram combined with clinical features

We combined the clinical factors of age, albuminuria and radiomics score (Rad-Score) to construct a radiomics nomogram. As shown in **Fig 6**. Decision curve analysis (DCA) proves that between about 30% and about 90% of the high-risk threshold, both models can achieve better net benefits than all or none, but the value of the radiomics model higher (**Fig 7**). The calibration curve shows the goodness of fit of the nomogram. The 45° dashed line represents the ideal prediction model, and the black line represents the prediction performance of the nomogram (**Fig 8**). The closer the black line is to the ideal prediction line, the better the prediction effect of the model. In order to better apply the radiomics model to the clinic and improve the accuracy of the model, we combined the clinical model with the radiomics model to draw a nomogram of the comprehensive model (radiomics + clinical) to make the model more intuitive. Considering that the construction of the model involves 11 radiomics features, in order to simplify the model, we reduce the dimensions of 11 image parameters and express them with Rad-Score. Rad-Scores are calculated using the following formula:

Rad-scores= Log-sigma-1-0-mm-3D_glcm_Autocorrelation*1.03823

+Log-sigma-1-5-mm-3D_firstorder_Kurtosis*-0.11197

+Log-sigma-2-0-mm-3D_glcm_JointAverage*0.12997

+Log-sigma-2-5-mm-3D_gldm_LowGrayLevelEmphasis*-0.38671

+Wavelet-LHH_glcm_Autocorrelation*-1.72581

+Wavelet-LHH_glszm_SmallAreaHighGrayLevelEmphasis*-0.88659

+Wavelet-LHL_gldm_LargeDependence*0.45270

+Wavelet-LLH_glcm_JointAverage*3.25086

+Original_shape_MajorAxisLength*-0.05676

+Original_shape_MinorAxisLength*0.57564

+Original_shape_Maximum2DDiameterSlice*0.87998

Discussion

The pathological grade of bladder cancer is closely related to the choice of treatment and prognosis. Cystoscopy has the risk of urinary tract infection, injury and implant transfer, and the misdiagnosis rate is high (48–49). At present, artificial intelligence and texture analysis technology are used from image data to mine a large number of texture features that are specifically related to the interior of the tumor, providing clinical and radiologists with in-depth information that cannot be obtained from conventional images, and assisting them in diagnosing and predicting tumor features. It has become the main hot direction of current research, especially showing strong potential in the clinical diagnosis and prediction of bladder cancer. Relevant studies at home and abroad have confirmed that radiological features have good performance in the prognosis of bladder cancer and the identification of muscle invasion (39, 41). Previous studies have shown that by comparing the texture information of dynamic enhanced magnetic resonance imaging (DCE MRI) and diffusion weighted imaging (DWI) of patients with bladder cancer, it is found that the DCE-MRI sequence has certain significance in identifying recurrence and inflammation after bladder cancer. Further research it is found that the DCE-MRI sequence also has better performance in the differentiation of bladder cancer and glandular cystitis (39–40). Numerous studies and analyses have shown that MRI has applications in the pathological grading and diagnosis of bladder cancer due to its high resolution (50). However, MRI has the advantages of long time, high economic cost, and many scanning parameters, while CT has short time and low cost. Thin-slice CT enhanced images can show the lesions more clearly, and it is not easy to cause the omission of edge texture information. At the same time, CT texture features can reflect the distribution characteristics of focal cells and contrast agents in the intracellular and external intercellular spaces of blood vessels, non-invasively quantify the tumor microenvironment, evaluate the heterogeneity of the tumor, and provide help for the formulation of clinical treatment plans (51). Previous studies have shown that CT texture technology can diagnose and predict the pathological grade of bladder cancer, but it does not incorporate clinical features, the diagnosis mode is relatively simple, cannot be displayed in the form of a nomogram, and the sample size is small (52–53). Therefore, we propose a new radiological biomarker to assess the preoperative pathological grading of bladder cancer, and construct a predictive model in conjunction with clinical practice. The results show that CT-based radiomics features, combined with machine learning algorithms and clinical features, can better distinguish HGUC and LGUC.

Construct and verify the radiomics features based on multi-parameter thin-layer enhanced CT to predict the preoperative pathological grading of patients with bladder cancer. In addition, we have developed a predictive nomogram, which includes radiological characteristics and clinical risk factors. Therefore, this research mainly cuts into the subject from two perspectives and starts the research: (1) Constructing a prediction model of bladder tumor pathological grading based on multi-parameter thin-layer enhanced CT image features for preoperative prediction. (2) Construct a pathological prediction model based on logistic regression, and combine clinical related factors to construct a comprehensive prediction model of (radiomics + clinical), which greatly enhances the comprehensive performance of the bladder cancer pathological grading prediction model. In this study, we used different learning algorithms and compared the pros and cons of each algorithm.

The logistic regression model has the best performance. In the end, we initially established a radiomics model based on CT images to predict the pathological grade of bladder cancer. In order to effectively solve the problem that different gray level differences between different thin-slice CTs have a serious impact on the texture feature extraction results, this research first outlines the entire tumor ROI in the original image data, and performs texture analysis on the ROI. In this study, we used a three-dimensional (3D) region of interest. Compared with using a two-dimensional (2D) region of interest, the resolution efficiency is improved, because the 3D ROI takes into account all available slices, and the entire tumor analysis seems to be larger than the maximum horizontal Cross-sectional area can better indicate tumor heterogeneity (54). Then, texture features were extracted from the GLDM, GLCM, GLRLM, GLSZM, NGDTM, First-order and Shape features in the tumor ROI with a specific gray level, and a total of 1223 radiomics features were extracted. Considering that there are many features involved in research and selection, it is easy to cause the model's predictive performance to overfit, which will affect the comprehensive ability and generalization ability of the radiomics model. Therefore, based on the extracted 1223 features, this study uses lasso regression to select the optimal feature subset, and finally obtains 11 radiomics features to quantitatively describe the image difference between HGUC and LGUC, and improve the comprehensive performance of the prediction model. The results show that the optimal features selected by the above feature selection method increase the model's prediction accuracy of bladder cancer pathological grading to 79.15%, and the C-index is 0.858. Two of these 11 optimal features are GLDM features, which shows that GLDM features based on the gray-scale dependence of quantified images are more effective in quantifying the heterogeneous difference between HGUC and LGUC. There are four GLDM features, one GLSZM feature, the First-order and Shape features. These texture features can effectively reflect the internal differences between HGUC and LGUC.

In this study, the radiomics features were selected from the training group through the selection operator (LASSO) regression method. The 11 effective features that constitute the radiomics label represent different texture characteristics in the image and reflect the unevenness of the internal tissue of the tumor tissue. Independent sample T test and rank sum test showed that "Autocorrelation" and "Joint-Average" in the second-order feature gray level co-occurrence matrix (GLCM) were correlated with high and low levels of bladder cancer ($p < 0.0001$). Autocorrelation is a measure of texture fineness and roughness. The joint average (Joint-Average) represents the returned average grayscale intensity distribution. Studies have shown that autocorrelation is closely related to tumor invasion (55–56). The higher the autocorrelation value, the stronger the heterogeneity of the texture pattern (57). In our study, the autocorrelation value of high-grade urothelial carcinoma was significantly greater than that of low-grade urothelial carcinoma. It can be concluded that the higher the autocorrelation value of bladder tumors, the higher the pathological grade ($p < 0.0001$). In addition, the "kurtosis" in the first-order feature is the "peak" measure of the average distribution of the image ROI. Related studies have shown that kurtosis is related to the invasion of cervical cancer and the invasion of the muscle layer of the bladder (58–60). In our study, larger kurtosis values may represent high-grade tumors. In addition, the gray-level dependent matrix parameters "LowGrayLevelEmphasis" and "LargeDependenceLowGrayLevelEmphasis" in the high-level features are also closely related to the pathological grading of bladder tumors. The LowGrayLevelEmphasis represents the distribution of low gray values, and a higher value indicates a greater concentration of low gray values in the image. The study found that the larger the key value of the low gray level, the more the tumor tends to be low-level. Large Dependence Low Gray Level Emphasis represents the joint distribution of large dependencies with lower gray values. The larger the value, the more likely the tumor is to be high-grade urothelial carcinoma. Through research, we also found that the shape feature in the texture feature also has a certain relationship with the pathological grade of bladder tumor. Among them, the Maximum2DDiameterSlice, MajorAxisLength and MinorAxisLength are all parameters of the tumor size. As the diameter of the tumor increases, the pathological grade will also increase. Among the four models, the model based on the logistic regression algorithm has the best comprehensive effect, and the comprehensive performance of the accuracy, specificity and AUC value of the logistic regression model is the best. In the training group, the radiomics model based on logistic regression has accuracy, sensitivity, specificity and AUC values of 79.15%, 75.40%, 82.71% and 0.858, respectively. In the verification group, its accuracy, sensitivity, specificity and AUC value were 72.57%, 76.36%, 68.97% and 0.800, respectively.

Comprehensive comparison of each model, the overall performance of the radiomics model based on logistic regression is better.

Compared with the models established in previous studies, we combine the relevant clinical indicators on the basis of the radiomics model, so that the model can be better applied to the clinic and has better diagnostic performance. This may be because we have used radiomics to extract a large number of features from the original image and the filtered image, or it may be that we have fully excavated clinically relevant factors. This study found that age and albuminuria are related to pathological grading through univariate analysis and multivariate analysis, which are independent risk factors for pathological grading ($p < 0.001$). There is advanced age and albuminuria before surgery, and postoperative pathology is high-grade urothelium. The probability of cancer is greatly increased. In addition, the larger the tumor diameter, the greater the probability of high-grade urothelial carcinoma, which coincides with the results obtained by the shape parameters in the radiomics texture feature. In this study, a clinical prediction model was established by combining the clinical characteristics of age and albuminuria. The AUC value of the clinical model established on this basis is 0.650, and the AUC value of the radiomics model is 0.858. Compared with the clinical model, the radiomics model obtained a higher AUC value in distinguishing HGUC from LGUC (0.858 training group = 0.858 and verification group = 0.800), and the radiomics model is better in terms of the predictive ability of the model, in order to further improve the prediction ability of the model, and adding clinical factors, we constructed a radiomics-clinical prediction model (AUC = 0.866), and developed a nomogram, which has a good prediction value for distinguishing HGUC from LGUC. Then verify and calibrate it. The calibration curve and decision curve can well verify that the radiomics-clinical model has better predictive performance. In addition, the HGUC (190 cases) and LGUC (182 cases) sample distributions in this study are more balanced. This model can effectively suppress the prediction bias caused by sample imbalance and effectively enhance the predictive ability of pathological classification. There is also a big bright spot in this study. The traditional prediction model is inconvenient to use. In order to make the model better applied to the clinic, we have drawn the prediction model nomogram. Clinicians can intuitively and conveniently use the model to make effective clinical predictions. The results of this study show that the combination of multi-parameter thin-layer enhanced CT radiomics features and clinical can quantitatively characterize the pathological grading of patients with bladder cancer, which has important clinical application value.

The novelty of this study can be summarized as follows: (1) This is the first use of multi-parameter thin-layer enhanced CT imaging to predict the pathological grading of bladder tumors before surgery; (2) Using image texture features and three-dimensional region of interest ROI reflect the intensity and spatial changes of different atlases to better characterize the heterogeneity of tumors; (3) Sample rebalance and feature selection methods are used together to enhance prediction performance. (4) Combining clinically specific factors to construct radiomics-clinical prediction model, and develop a prediction nomogram.

Radiomics features based on multi-parameter thin-layer enhanced CT have great potential in predicting the pathological grading of bladder cancer. In addition, this study is a retrospective analysis and still has certain limitations. In addition, the study only conducted a study on one center, lacking comparison and generalization, retrospective design may introduce selection bias, and the diffusion of CT-enhanced contrast agents may exist in individual difference. In follow-up studies, we will conduct multi-center studies, even prospective, and we will continue to collect more CT data from eligible patients in the future to establish a more comprehensive and more efficient diagnostic predictive model.

In summary, this study constructed a radiomics model based on multi-parameter thin-layer enhanced CT to predict the pathological grade of bladder cancer. The model has good diagnostic efficiency, can distinguish high-grade and low-grade bladder cancer, and draws a nomogram, which makes it more intuitive and convenient for clinicians to use, and provides help for the diagnosis and treatment of bladder cancer.

Abbreviations

ROI	Region of interest
ICC	Inter-/intra- class correlation coefficient
LASSO	Least absolute shrinkage and selection operator
C-index	conformance index
ROC	Receiver operator characteristic
DCA	Decision curve analysis
BCa	Bladde Cancer
NMIBC	non-muscle invasive bladder cancer
MIBC	muscle invasive bladder cancer
HGUC	High-grade urothelial carcinoma
LGUC	low-grade urothelial carcinoma
DCE-MRI	dynamic contraction-enhanced magnetic resonance imaging
PET	positron emission tomography
CT	Computerized tomography
MS	metabolic syndrome
HBP	high blood pressure
BMI	body mass index
HDL-C	high-density lipoprotein
DM	diabetes mellitus
TG	Triglyceride
PACS	picture archiving and communication system
DICOM	digital imaging and communications in medicine
GLRLM	gray-level run-length matrix
GLDM	gray-level dependence matrix
GLSZM	gray-level size zone matrix
NGTDM	neighboring gray-tone difference matrix
GLCM	gray-level co-occurrence matrix
3D	three-dimensional
AUC	area under the curve
SVM	support vector machine
Rad-score	Radiomics score
CI	Confidence interval

Declarations

Ethics approval and consent to participate: All procedures performed in studies involving human participants were in accordance with the ethical standards of the institutional and national research committee. The Ethics Committee of the First Affiliated Hospital of Soochow University approved the study.

Consent for publication: yes

Availability of data and material: All the original data of this study can be made public and can be provided at any time as needed.

Conflicts of Interest: All authors have completed the ICMJE uniform disclosure form. The authors have no conflicts of interest to declare. Conflict of interest relevant to this article was not reported.

Funding

This work was supported by the Suzhou Science and Techonology Project (SLJ201906 and SYS2019053).

Authors' contributions: (I) Conception and design: Qi Zhou*, Jun Ouyang; (II) Administrative support: Caiping Mao, Zhiyu Zhang, Jun Ouyang; (III) Provision of study materials or patients: Qi Zhou*, Lu Ma*, Haoyang Zhang*, Xiaojie Ang, Can Hu; (IV) Collection and assembly of data: Qi Zhou*, Lu Ma*, Haoyang Zhang*, Xiaojie Ang, Can Hu; (V) Data analysis and interpretation: Qi Zhou*, Lu Ma*, Haoyang Zhang*, Xiaojie Ang, Can Hu; (VI) Manuscript writing: All authors; (VII) Final approval of manuscript: All authors.

*These authors contributed equally to this work.

Acknowledgements: None.

Code availability: All the codes involved in this study are submitted with the article and can be made public.

Ethics approval: The author is responsible for all aspects of the work to ensure that issues related to the accuracy or completeness of any part of the work are properly investigated and resolved. The study is based on the Helsinki Declaration (JAMA 2000; 284:3043–3049). The study was approved by the Ethics Committee of the first affiliated Hospital of Suzhou University and obtained the informed consent of all participants.

References

1. Siegel RL, Miller KD, Jemal A. Cancer statistics, 2019. CA Cancer J Clin. 2019;69(1):7–34.
2. Kamat AM, Hahn NM, Efstathiou JA, et al. Bladder cancer. Lancet. 2016;388(10061):2796–810.
3. Pang C, Guan Y, Li H, et al. Urologic cancer in China. Jpn J Clin Oncol. 2016;46(6):497–501.
4. Berdik C. Unlocking bladder cancer. Nature. 2017;551(7679):S34-s5.
5. Chen W, Zheng R, Baade PD, et al. Cancer statistics in China, 2015. CA Cancer J Clin. 2016;66(2):115–32.
6. Humphrey PA, Moch H, Cubilla AL, et al. The 2016 WHO Classification of Tumours of the Urinary System and Male Genital Organs-Part B: Prostate and Bladder Tumours. Eur Urol. 2016;70(1):106–19.
7. Rouprêt M, Babjuk M, Compérat E, et al. European Association of Urology Guidelines on Upper Urinary Tract Urothelial Carcinoma: 2017 Update. Eur Urol. 2018;73(1):111–22.
8. Fiuk JV, Schwartz BF. Upper tract urothelial carcinoma: Paradigm shift towards nephron sparing management. World J Nephrol. 2016;5(2):158–65.
9. Klaassen Z, Kamat AM, Kassouf W, et al. Treatment Strategy for Newly Diagnosed T1 High-grade Bladder Urothelial Carcinoma: New Insights and Updated Recommendations. Eur Urol. 2018;74(5):597–608.

10. Leblanc B, Duclos AJ, Bénard F, et al. Long-term followup of initial Ta grade 1 transitional cell carcinoma of the bladder. J Urol. 1999;162(6):1946–50.
11. Palou J, Sylvester RJ, Faba OR, et al. Female gender and carcinoma in situ in the prostatic urethra are prognostic factors for recurrence, progression, and disease-specific mortality in T1G3 bladder cancer patients treated with bacillus Calmette-Guérin. Eur Urol. 2012;62(1):118–25.
12. Gudjónsson S, Adell L, Merdasa F, et al. Should all patients with non-muscle-invasive bladder cancer receive early intravesical chemotherapy after transurethral resection? The results of a prospective randomised multicentre study. Eur Urol. 2009;55(4):773–80.
13. Babjuk M, Böhle A, Burger M, et al. EAU Guidelines on Non-Muscle-invasive Urothelial Carcinoma of the Bladder: Update 2016. Eur Urol. 2017;71(3):447–61.
14. Hansel DE, Amin MB, Comperat E, et al. A contemporary update on pathology standards for bladder cancer: transurethral resection and radical cystectomy specimens. Eur Urol. 2013;63(2):321–32.
15. Lambin P, Petit SF, Aerts HJ, et al. The ESTRO Breur Lecture 2009. From population to voxel-based radiotherapy: exploiting intra-tumour and intra-organ heterogeneity for advanced treatment of non-small cell lung cancer. Radiother Oncol. 2010;96(2):145 – 52.
16. Atri M. New technologies and directed agents for applications of cancer imaging. J Clin Oncol. 2006;24(20):3299–308.
17. Ehman RL, Hendee WR, Welch MJ, et al. Blueprint for imaging in biomedical research. Radiology. 2007;244(1):12–27.
18. Hillman BJ. Introduction to the special issue on medical imaging in oncology. J Clin Oncol. 2006;24(20):3223–4.
19. Ashamalla H, Rafla S, Parikh K, et al. The contribution of integrated PET/CT to the evolving definition of treatment volumes in radiation treatment planning in lung cancer. Int J Radiat Oncol Biol Phys. 2005;63(4):1016–23.
20. Belfiore G, Moggio G, Tedeschi E, et al. CT-guided radiofrequency ablation: a potential complementary therapy for patients with unresectable primary lung cancer–a preliminary report of 33 patients. AJR Am J Roentgenol. 2004;183(4):1003–11.
21. Brink I, Schumacher T, Mix M, et al. Impact of [18F]FDG-PET on the primary staging of small-cell lung cancer. Eur J Nucl Med Mol Imaging. 2004;31(12):1614–20.
22. Ciernik IF, Dizendorf E, Baumert BG, et al. Radiation treatment planning with an integrated positron emission and computer tomography (PET/CT): a feasibility study. Int J Radiat Oncol Biol Phys. 2003;57(3):853–63.
23. de Torres JP, Bastarrika G, Wisnivesky JP, et al. Assessing the relationship between lung cancer risk and emphysema detected on low-dose CT of the chest. Chest. 2007;132(6):1932–8.
24. Lee KS, Jeong YJ, Han J, et al. T1 non-small cell lung cancer: imaging and histopathologic findings and their prognostic implications. Radiographics. 2004;24(6):1617–36; discussion 32 – 6.
25. Lehman CD, Isaacs C, Schnall MD, et al. Cancer yield of mammography, MR, and US in high-risk women: prospective multi-institution breast cancer screening study. Radiology. 2007;244(2):381–8.
26. Nelson ED, Slotoroff CB, Gomella LG, et al. Targeted biopsy of the prostate: the impact of color Doppler imaging and elastography on prostate cancer detection and Gleason score. Urology. 2007;70(6):1136–40.
27. Paajanen H. Increasing use of mammography improves the outcome of breast cancer in Finland. Breast J. 2006;12(1):88–90.
28. Sarkeala T, Heinävaara S, Anttila A. Breast cancer mortality with varying invitational policies in organised mammography. Br J Cancer. 2008;98(3):641–5.
29. Eisenhauer EA, Therasse P, Bogaerts J, et al. New response evaluation criteria in solid tumours: revised RECIST guideline (version 1.1). Eur J Cancer. 2009;45(2):228–47.
30. Fass L. Imaging and cancer: a review. Mol Oncol. 2008;2(2):115–52.

31. Lambin P, Leijenaar RTH, Deist TM, et al. Radiomics: the bridge between medical imaging and personalized medicine. Nat Rev Clin Oncol. 2017;14(12):749–62.
32. Luo C, Huang B, Wu Y, et al. Use of Vesical Imaging-Reporting and Data System (VI-RADS) for detecting the muscle invasion of bladder cancer: a diagnostic meta-analysis. Eur Radiol. 2020;30(8):4606–14.
33. Wang H, Hu D, Yao H, et al. Radiomics analysis of multiparametric MRI for the preoperative evaluation of pathological grade in bladder cancer tumors. Eur Radiol. 2019;29(11):6182–90.
34. Shaikh F, Franc B, Allen E, et al. Translational Radiomics: Defining the Strategy Pipeline and Considerations for Application-Part 2: From Clinical Implementation to Enterprise. J Am Coll Radiol. 2018;15(3 Pt B):543–9.
35. Lu Y, Liu L, Luan S, et al. The diagnostic value of texture analysis in predicting WHO grades of meningiomas based on ADC maps: an attempt using decision tree and decision forest. Eur Radiol. 2019;29(3):1318–28.
36. Panebianco V, De Berardinis E, Barchetti G, et al. An evaluation of morphological and functional multi-parametric MRI sequences in classifying non-muscle and muscle invasive bladder cancer. Eur Radiol. 2017;27(9):3759–66.
37. van der Pol CB, Chung A, Lim C, et al. Update on multiparametric MRI of urinary bladder cancer. J Magn Reson Imaging. 2018;48(4):882–96.
38. Dercle L, Henry T, Carré A, et al. Reinventing radiation therapy with machine learning and imaging bio-markers (radiomics): State-of-the-art, challenges and perspectives. Methods. 2020.
39. Wang HJ, Pui MH, Guo Y, et al. Preliminary study of diffusion-weighted MRI in the preoperative diagnosis of cystitis glandularis. Clin Radiol. 2016;71(9):937.e1-4.
40. Wang HJ, Pui MH, Guo Y, et al. Diffusion-weighted MRI in bladder carcinoma: the differentiation between tumor recurrence and benign changes after resection. Abdom Imaging. 2014;39(1):135–41.
41. Xu X, Liu Y, Zhang X, et al. Preoperative prediction of muscular invasiveness of bladder cancer with radiomic features on conventional MRI and its high-order derivative maps. Abdom Radiol (NY). 2017;42(7):1896–905.
42. Xu X, Zhang X, Tian Q, et al. Three-dimensional texture features from intensity and high-order derivative maps for the discrimination between bladder tumors and wall tissues via MRI. Int J Comput Assist Radiol Surg. 2017;12(4):645–56.
43. Zhang X, Xu X, Tian Q, et al. Radiomics assessment of bladder cancer grade using texture features from diffusion-weighted imaging. J Magn Reson Imaging. 2017;46(5):1281–8.
44. Gillies RJ, Kinahan PE, Hricak H. Radiomics: Images Are More than Pictures, They Are Data. Radiology. 2016;278(2):563–77.
45. Lambin P, Rios-Velazquez E, Leijenaar R, et al. Radiomics: extracting more information from medical images using advanced feature analysis. Eur J Cancer. 2012;48(4):441–6.
46. Chicklore S, Goh V, Siddique M, et al. Quantifying tumour heterogeneity in 18F-FDG PET/CT imaging by texture analysis. Eur J Nucl Med Mol Imaging. 2013;40(1):133–40.
47. Mu W, Chen Z, Liang Y, et al. Staging of cervical cancer based on tumor heterogeneity characterized by texture features on (18)F-FDG PET images. Phys Med Biol. 2015;60(13):5123–39.
48. Jakse G, Algaba F, Malmström PU, et al. A second-look TUR in T1 transitional cell carcinoma: why? Eur Urol. 2004;45(5):539–46; discussion 46.
49. Miladi M, Peyromaure M, Zerbib M, et al. The value of a second transurethral resection in evaluating patients with bladder tumours. Eur Urol. 2003;43(3):241–5.
50. Cai W, Li F, Wang J, et al. A comparison of arterial spin labeling perfusion MRI and DCE-MRI in human prostate cancer. NMR Biomed. 2014;27(7):817–25.
51. Ng F, Ganeshan B, Kozarski R, et al. Assessment of primary colorectal cancer heterogeneity by using whole-tumor texture analysis: contrast-enhanced CT texture as a biomarker of 5-year survival. Radiology. 2013;266(1):177–84.

52. Mammen S, Krishna S, Quon M, et al. Diagnostic Accuracy of Qualitative and Quantitative Computed Tomography Analysis for Diagnosis of Pathological Grade and Stage in Upper Tract Urothelial Cell Carcinoma. J Comput Assist Tomogr. 2018;42(2):204–10.
53. Zhang G, Xu L, Zhao L, et al. CT-based radiomics to predict the pathological grade of bladder cancer. Eur Radiol. 2020;30(12):6749–56.
54. Ng F, Kozarski R, Ganeshan B, et al. Assessment of tumor heterogeneity by CT texture analysis: can the largest cross-sectional area be used as an alternative to whole tumor analysis? Eur J Radiol. 2013;82(2):342–8.
55. Dodington DW, Lagree A, Tabbarah S, et al. Analysis of tumor nuclear features using artificial intelligence to predict response to neoadjuvant chemotherapy in high-risk breast cancer patients. Breast Cancer Res Treat. 2021.
56. Yu H, Meng X, Chen H, et al. Correlation Between Mammographic Radiomics Features and the Level of Tumor-Infiltrating Lymphocytes in Patients With Triple-Negative Breast Cancer. Front Oncol. 2020;10:412.
57. Liu S, Zheng H, Zhang Y, et al. Whole-volume apparent diffusion coefficient-based entropy parameters for assessment of gastric cancer aggressiveness. J Magn Reson Imaging. 2018;47(1):168–75.
58. Azehoun-Pazou GM, Assogba KM, Adegbidi H, et al. Characterisation of black skin stratum corneum by digital macroscopic images analysis. Healthc Technol Lett. 2020;7(6):161–7.
59. Li Q, Cao B, Tan Q, et al. Prediction of muscle invasion of bladder cancer: A comparison between DKI and conventional DWI. Eur J Radiol. 2021;136:109522.
60. Zhang Q, Yu X, Ouyang H, et al. Whole-tumor texture model based on diffusion kurtosis imaging for assessing cervical cancer: a preliminary study. Eur Radiol. 2021.

Figures

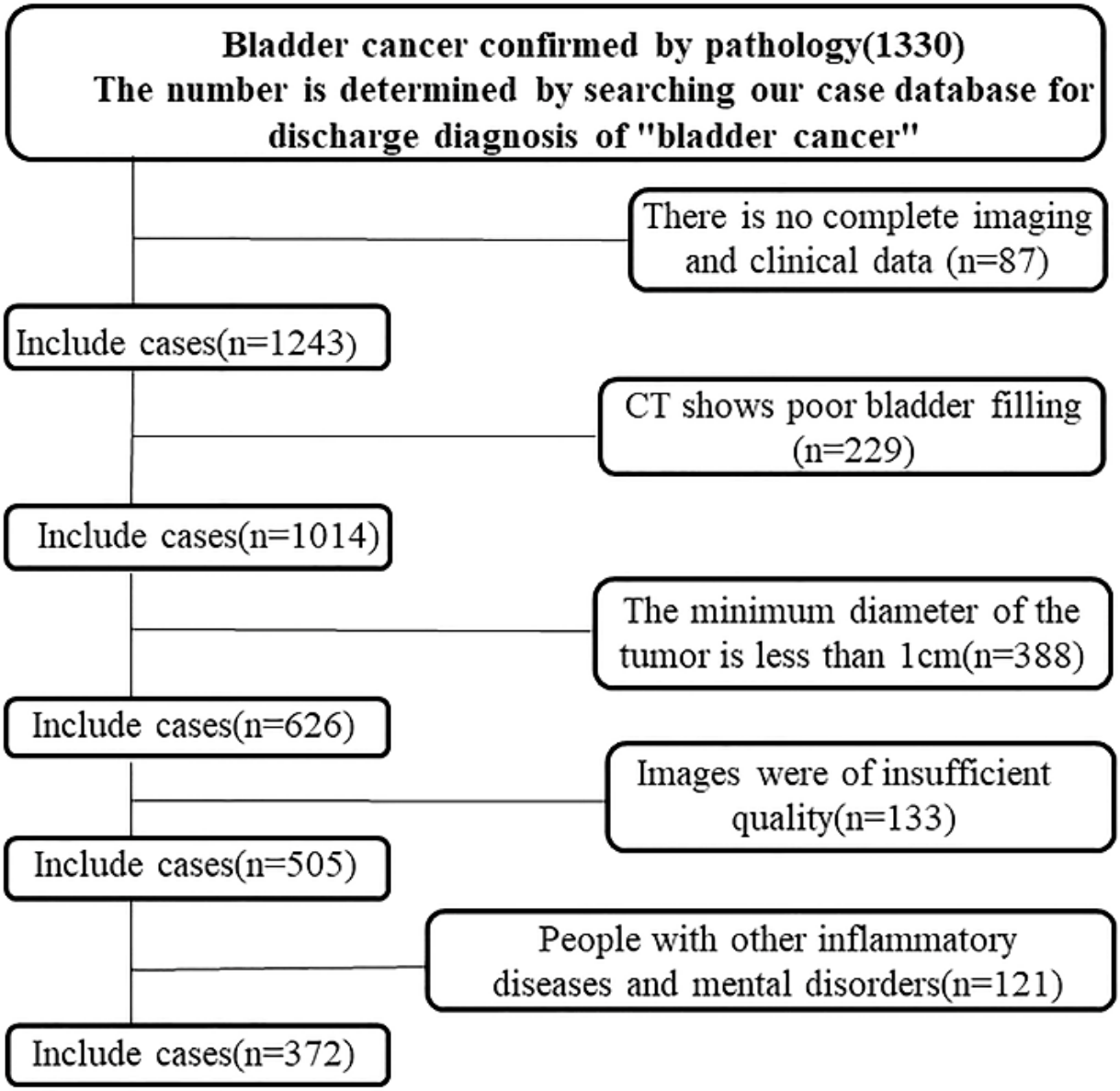

Figure 1

We screened 372 bladder cancer patients who met the research criteria through our hospital's case retrieval system and PACS imaging system.

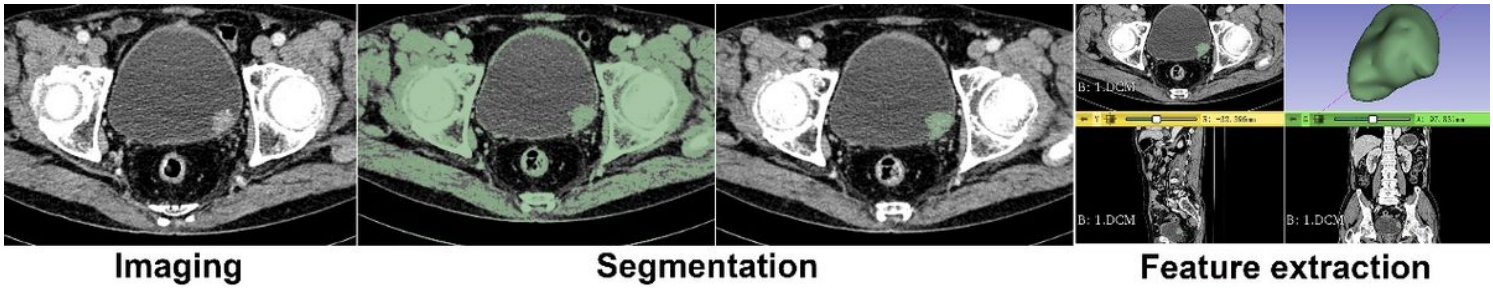

Figure 2

Semi-manual three-dimensional segmentation of the tumor, the tumor in 3D form, and the cutting of the tumor for smoothing.

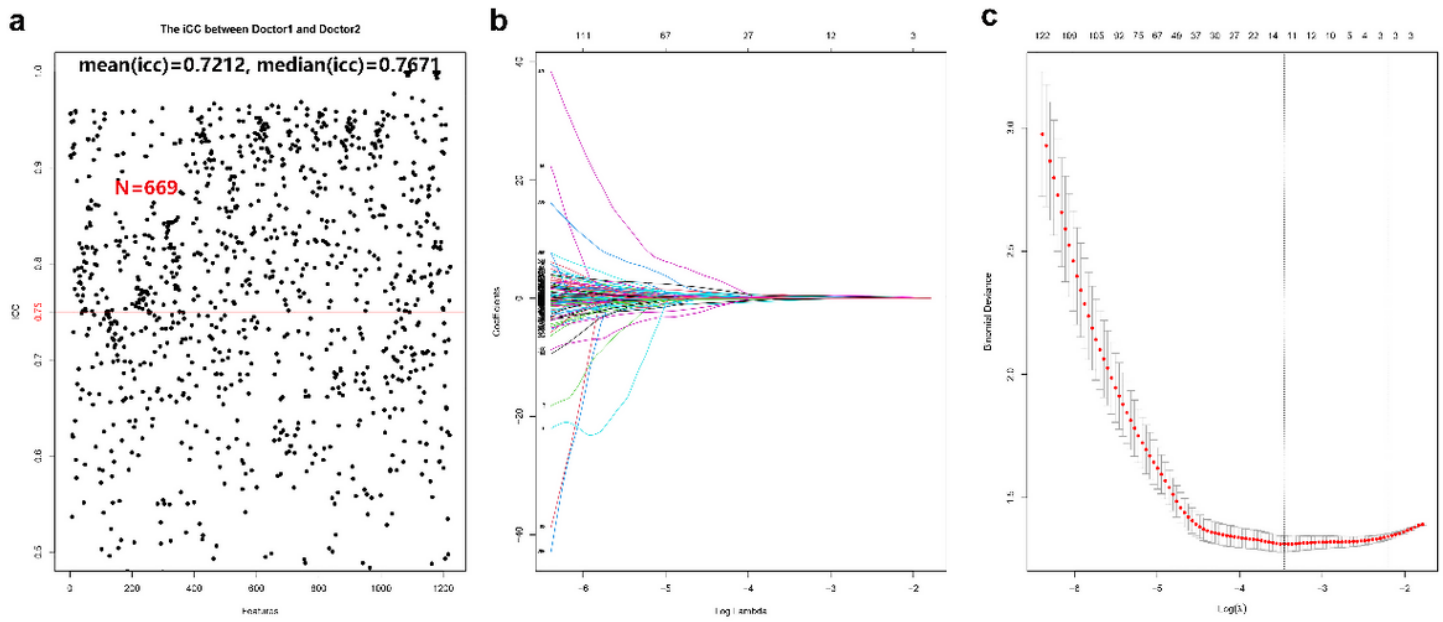

Figure 3

669 radiomic features proved to have good inter-group and intra-group consistency (a). Cross-validation is used to filter the coefficient of each feature at the best logarithm (λ). As the value of λ increases, the number of features becomes less and less (b). Use cross-validation to generate coefficients corresponding to the logarithmic (λ) value (minimum variance). Draw vertical lines with 11 selected radiological features (c).

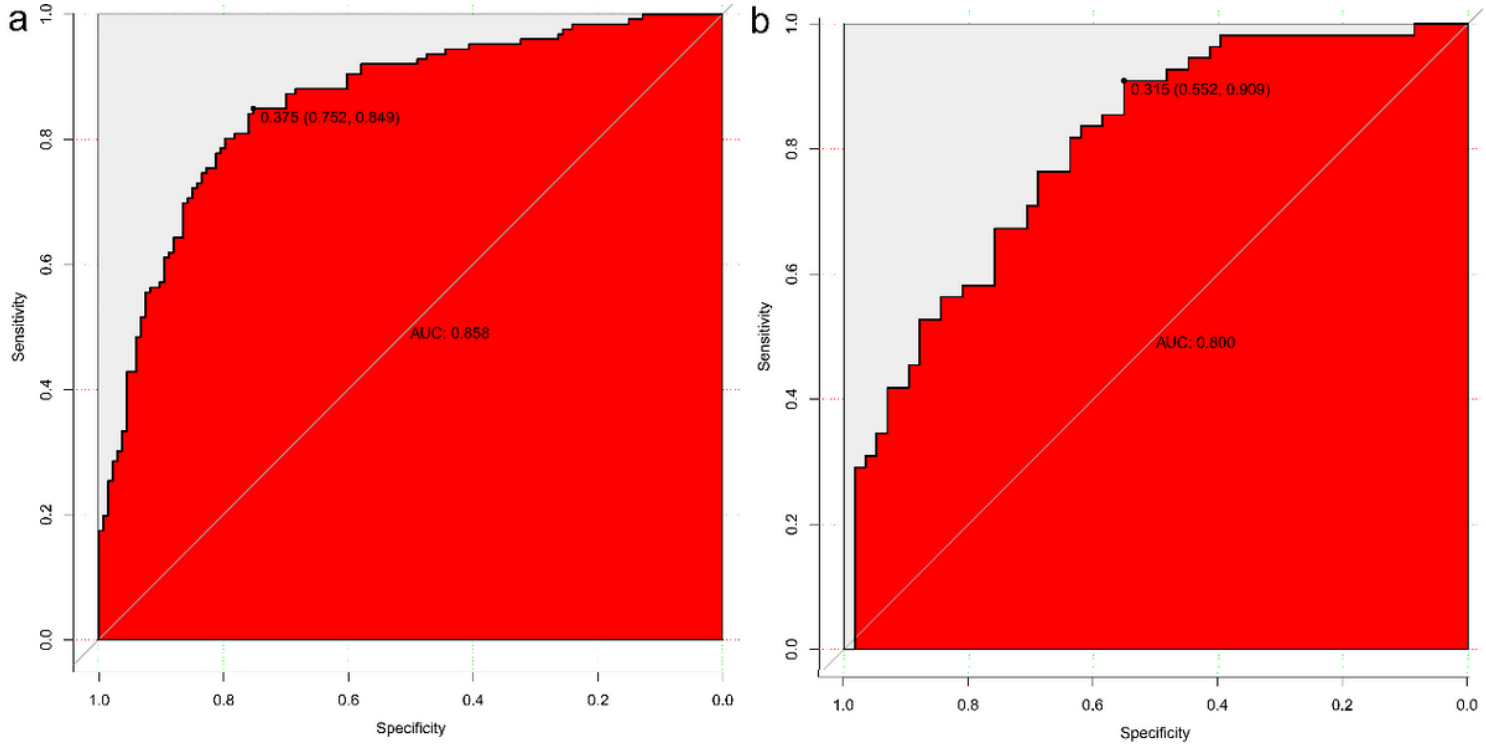

Figure 4

We build four prediction models on the basis of the training group. Comprehensive comparison shows that the logistic regression algorithm has the best diagnostic effect. The AUC values of the training group and the verification group are 0.858 (a) and 0.800 (b), respectively, and the overall performance is better.

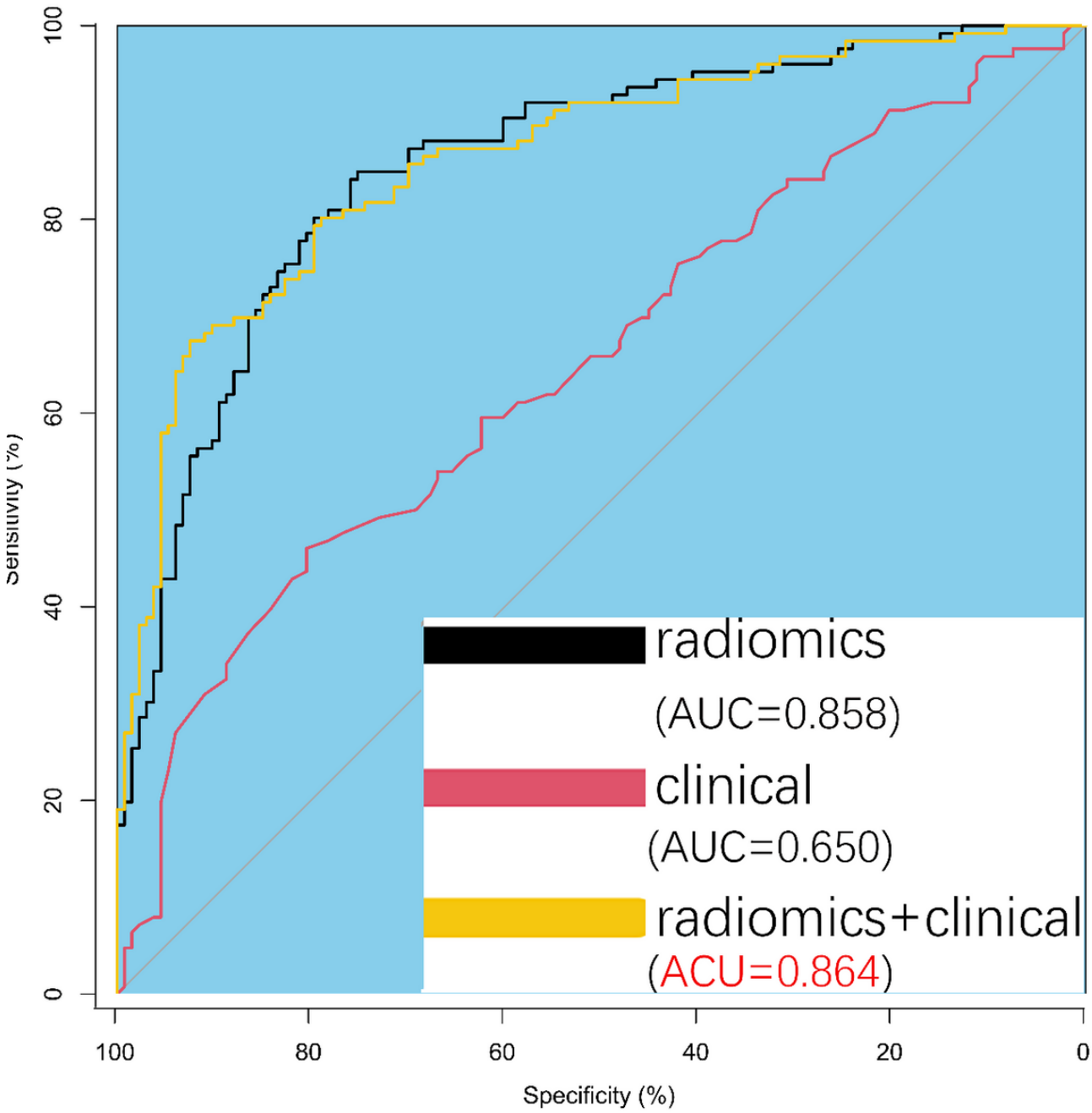

Figure 5

Comparing the ROC curves of the three models, there is a significant difference in the ROC between the radiomics model and the clinical model, while the radiomics model is not much different from the comprehensive model that combines clinical factors, and the efficiency of the comprehensive model is slightly better than that of the radiomics group model.

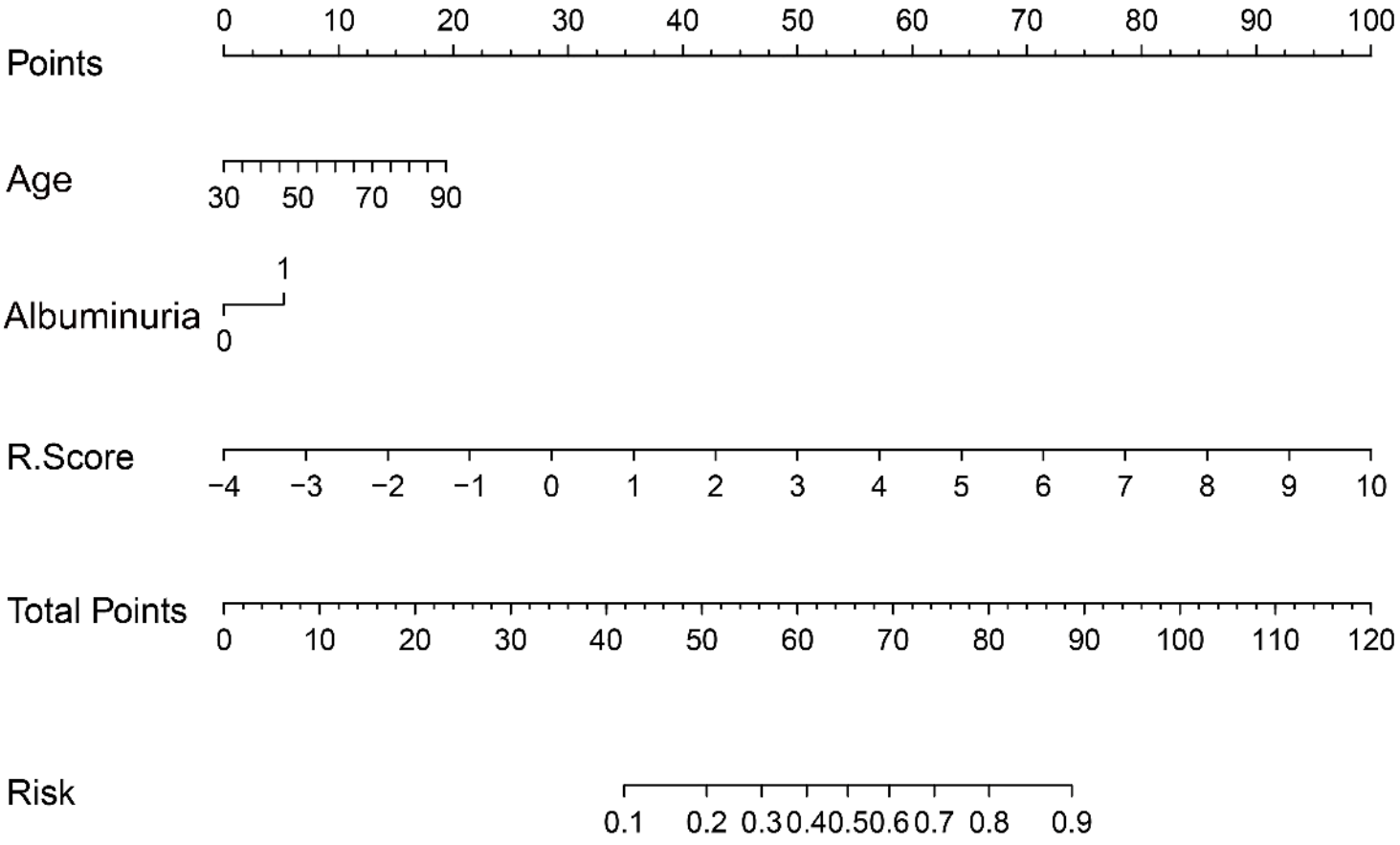

Figure 6

The nomogram can predict the probability of clinically high-grade urothelial carcinoma. Note: Each variable is located on its axis. Draw each vertical line up to the "score" axis to determine the score attributed to each variable. Sum the score of each variable and position it on the "Total Score" axis. Draw a vertical line to find the possibility of having high-grade urothelial cancer.

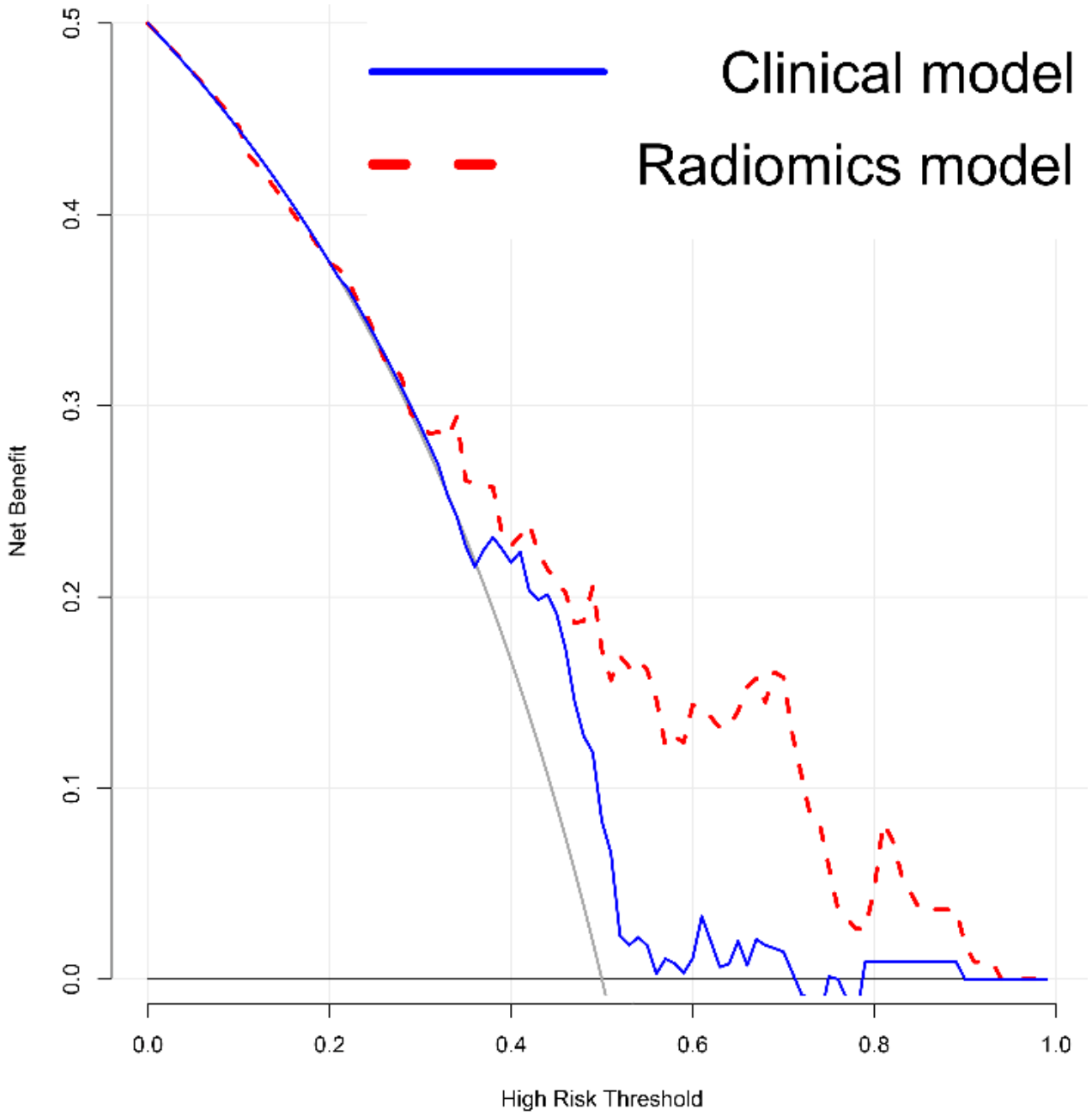

Figure 7

The red and blue lines represent the net benefits of radiological characteristics and clinical risk factors, respectively. The DCA curve proves that between the high-risk thresholds of about 30% and about 90%, both models can achieve better net benefits than all or none, but the radiomics model is more valuable.

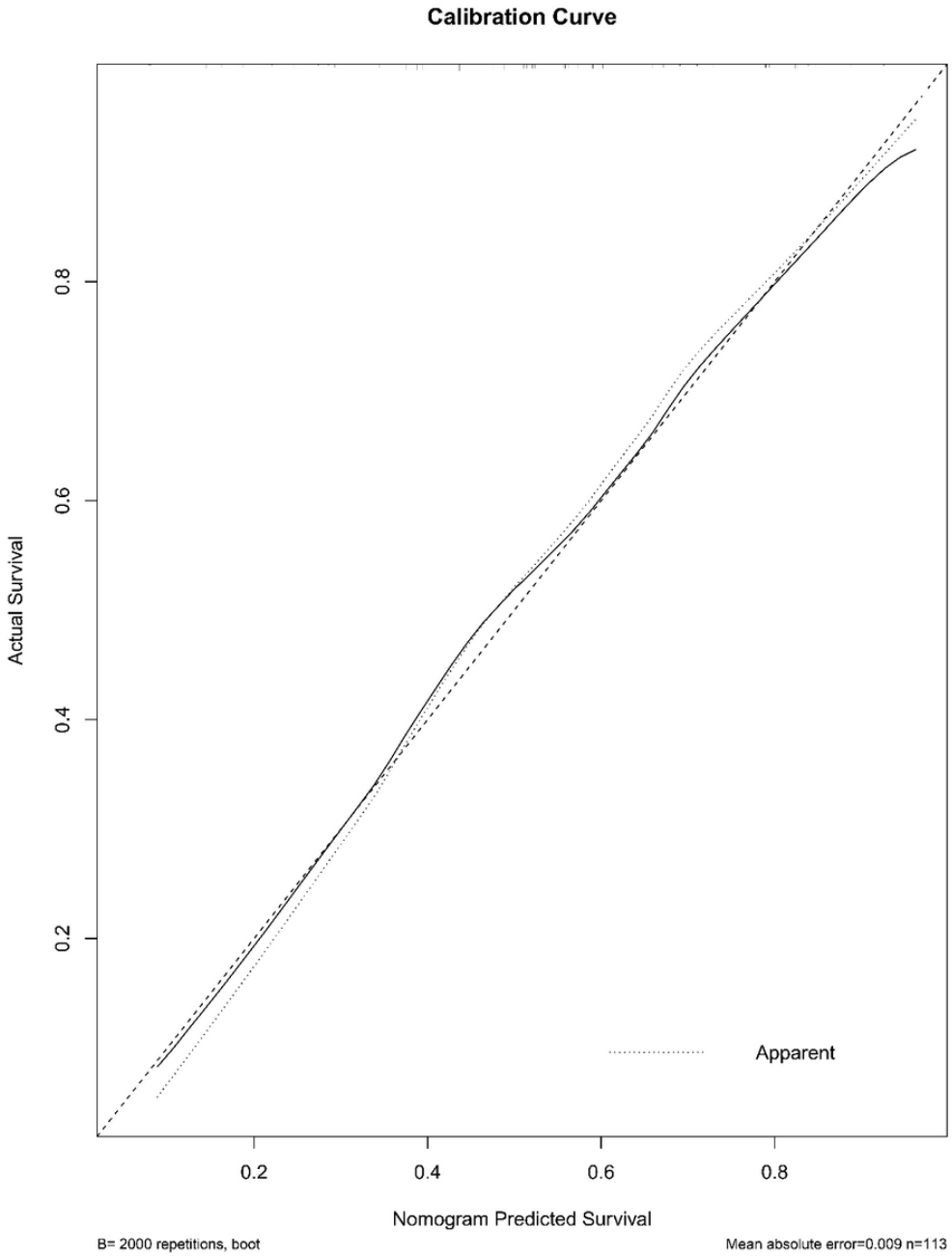

Figure 8

The calibration curve of the nomogram. Obviously, the curve represents the relationship between the predicted probability and the actual probability of clinically significant high-grade urothelial cancer based on our entire study population. 2,000 resampling are used to draw a deviation correction curve through bootstrapping. The ideal curve is a 45° line, which means perfect predictions can be made.